



Analysis of thermal stability and pyrolysis kinetic of dibutyl phosphate-based ionic liquid through thermogravimetry, gas chromatography/mass spectrometry, and Fourier transform infrared spectrometry

Hui-Chun Jiang¹ · Wei-Cheng Lin² · Min Hua^{1,3} · Xu-Hai Pan^{1,3} · Chi-Min Shu^{4,5} · Jun-Cheng Jiang^{1,3}

Received: 24 January 2018 / Accepted: 30 March 2019 / Published online: 11 April 2019
© Akadémiai Kiadó, Budapest, Hungary 2019

Abstract

To analyze the feasibility of phosphorus-containing ionic liquids used as flame retardants on flammable materials, thermal stability and pyrolysis kinetics of 1-butyl-3-methylimidazolium dibutyl phosphate ([Bmim][DBP]) were investigated using nonisothermal thermogravimetry. The apparent onset decomposition temperature (T_0) and mass fraction of residual carbon were 275.2–297.3 °C (± 0.5 °C) and 8.6–10.2% ($\pm 0.1\%$), respectively. The apparent activation energy (E_a), pre-exponential factor (A), and most probable kinetic function [$G(\alpha)$] were calculated using thermokinetic methods as $E_a = 152\text{--}164$ kJ mol⁻¹ (± 2 kJ mol⁻¹), $\ln A = 27.7 \pm 0.4$ s⁻¹, and $G(\alpha) = -\ln(1 - \alpha)$. The maximum operation temperature was estimated as 166.0 ± 0.2 °C, which was considerably lower than T_0 . The pyrolysis products were identified through gas chromatograph/mass and Fourier transform infrared spectrometers. As a novel finding, the main flame-retarding mechanism of [Bmim][DBP] occurred primarily in condensed phase. Complementally, [Bmim][DBP] was testified to have the flame-retardant effect on epoxy resin by limited oxygen index and vertical burning tests.

Keywords Phosphorus-containing ionic liquid · Pyrolysis kinetics · Maximum operation temperature · Pyrolysis products · Flame-retardant effect

List of symbols

A	Pre-exponential factor (s ⁻¹)
α	Fraction of conversion (mass%)
β	Heating rate (K min ⁻¹)
C	Constant
$C_{0.25}$	Reaction order, $n = 0.25$
C_1	First-order reaction
C_3	Reaction order, $n = 3$

$d\alpha/dt$	Mass loss rate (mass% min ⁻¹)
$(d\alpha/dt)_{0.5}$	Mass loss rate at the conversion of 0.5 (mass% min ⁻¹)
D_2	Valensi reaction
D_3	Jander reaction
3D	Z–L–T reaction
E_a	Apparent activation energy (kJ mol ⁻¹)
$f(\alpha)$	Most probable kinetic function
$G(\alpha)$	Integral mechanism function
[Him] ⁺	1 H-imidazole
$\ln A$	Logarithmic pre-exponential factor (s ⁻¹)
m	Fraction of mass residual (mass%)
m/z	Mass charge ratio (°C)

✉ Xu-Hai Pan
xuhaipan@163.com

✉ Chi-Min Shu
shucm@yuntech.edu.tw

¹ College of Safety Science and Engineering, Nanjing Tech University, Nanjing 210009, Jiangsu Province, China

² Graduate School of Engineering Science and Technology, National Yunlin University of Science and Technology (YunTech), 123, University Rd., Sec. 3, Douliou 64002, Yunlin, Taiwan, ROC

³ Jiangsu Key Laboratory of Hazardous Chemical Safety and Control, Nanjing 210009, Jiangsu Province, China

⁴ Center for Process Safety and Industrial Disaster Prevention, School of Engineering, YunTech, 123, University Rd., Sec. 3, Douliou, Yunlin, Taiwan, ROC

⁵ Department of Safety, Health, and Environmental Engineering, YunTech, 123, University Rd, Sec. 3, Douliou, Yunlin, Taiwan, ROC

[MHim] ⁺	3-Methyl-1 H-imidazole
[Mim] ⁺	Methyl imidazole
MOT	Maximum operation temperature (°C)
MOT _{1.0%}	Mass loss less than 1.0% of MOT (°C)
<i>R</i>	Universal gas constant (8.314 J mol ⁻¹ K ⁻¹)
<i>R</i> ²	Regression coefficient
<i>t</i>	Time of reaction (min)
<i>T</i>	Temperature (°C)
<i>T</i> _{0.5}	Temperature at the conversion of 0.5 (°C)
<i>T</i> _{ed}	End temperature (°C)
<i>T</i> _m	Maximum temperature (°C)
<i>T</i> ₀	Apparent onset decomposition temperature (°C)
<i>T</i> _p	Peak temperature (°C)
<i>y</i> ₁ (<i>α</i>)	Standard curve
<i>y</i> ₂ (<i>α</i>)	Experimental curve

Introduction

Ionic liquids (ILs) are organic molten salts at temperatures lower than 100 °C. They are entirely composed of cations and anions and have wide liquid range (e.g., [C₄mim][NTf₂]: - 89 to 450 °C) [1]. They have attracted immense interest because of their extraordinary properties, particularly high thermal stability, negligible vapor pressure, and nonflammability [2]. Moreover, ILs have been described as “designer solvents” because they can acquire various special properties if their constituent cations or anions are varied [3]. The use of specific ILs may improve the flame-retardant properties of polymers.

As an example of the most extensively used materials in various fields, conventional polymers such as polyurethane, polystyrene, polypropylene and epoxy resin have several useful properties. However, the inherent flammability of unmodified polymers largely prohibits their application in numerous crucial situations [4, 5]. Hence, reducing the flammability of polymers by adding flame retardants or grafting flame-retardant elements onto the polymers is necessary [6]. Historically, the use of nonhalogen flame retardants has been investigated. Phosphorus-containing flame retardants, considered to be the most promising halogen-free substitutes, have recently been favored by investigators [7, 8]. However, the flame-retardant efficiency of these phosphorus-containing retardants is low and large amounts of the retardants need to be added to the polymers for obtaining the desired effect. However, this addition deteriorates the mechanical properties of the polymers [9]. Hence, phosphorus-containing ILs have been suggested. Smaller amounts of the phosphate-containing

ILs are required; thus, these ILs have a higher flame-retardant efficiency. Such ILs efficiently enhance the flame-retardant properties of polymers by combining the advantages of phosphates and ILs [10].

Although studies have reported that some phosphorus-containing ILs markedly improve the flame-retardant properties of polymers, the thermal properties of these ILs have not been thoroughly explored. Moreover, the thermal stability, carbon-forming properties, pyrolysis mechanism, and decomposition products of ILs were reported to directly affect the mechanics and flame-retardant efficiency of the polymers to which they were added [11]. Therefore, investigating the thermal properties of ILs that could be used to modify polymers is necessary. In the literature, the short-term thermal stability of an IL is always characterized by its apparent onset decomposition temperature (*T*₀), peak temperature (*T*_p), and end temperature (*T*_{ed}), which are typically measured through ramped temperature thermogravimetry (TG) [12]. For instance, Ullah et al. [13] conducted ramped temperature TG to determine the short-term thermal stability of a benzimidazolium-based IL. Ramped temperature TG can preliminarily measure the carbon-forming tendency of ILs by observing the mass fraction of residual carbon.

The pyrolysis kinetic analysis of ILs is crucial in thermal analysis. However, studies typically calculate only the apparent activation energy (*E*_a) for a specific temperature range, which does not describe the entire thermal decomposition process. Moreover, pyrolysis kinetics is the paramount factor in effective process design [14, 15]. This study provided the complete and accurate calculation of the pyrolysis kinetics of an IL. It determined the precise *E*_a, pre-exponential factor (*A*), and most probable kinetic function [*G*(*α*)] using multiple kinetic models.

The short-term *T*₀, frequently used as an evaluation index, has been overestimated in the technical applications of ILs [16, 17]. In brief, although some ILs demonstrated remarkable thermal stability (high short-term *T*₀), as determined using nonisothermal TG, an enormous mass loss occurs in ILs long periods at low temperatures in isothermal TG [18, 19]. Thus, the maximum operation temperature (MOT) of ILs was proposed to represent their long-term thermal stability [20]. The MOT can be calculated using an empirical model, which has been verified to be accurate by Navarro et al. [21], and it has been widely used by other researchers [22].

Analysis of IL decomposition products is essential because some components of these products might affect the properties of modified composites [23]. Specifically, the suitability of an IL for improving the flame-retardant properties of polymers may depend strongly on whether its decomposition products are nontoxic and nonpolluting

[24]. In the present study, gas chromatograph/mass spectrometer (GC/MS) and Fourier transform infrared (FTIR) spectrometer were used to determine the components of the decomposition products.

In this study, the thermal properties of 1-butyl-3-methylimidazolium dibutyl phosphate ([Bmim][DBP]) were comprehensively investigated. First, its short-term thermal stability and carbon-forming property were measured using ramped temperature TG. Second, its pyrolysis kinetics [E_a , A , and $G(\alpha)$] were accurately calculated using various analysis methods. Moreover, the MOT was calculated using an empirical equation and compared with the analysis of isothermal TG curves. Finally, the decomposition products of [Bmim][DBP] were analyzed through GC/MS and FTIR spectrometers. In addition, relevant flame-retardant capacity of [Bmim][DBP] was also simply tested by the limited oxygen index (LOI) and vertical burning tests. In this study, we performed a preliminary analysis of the feasibility of [Bmim][DBP] as a flame retardant and provided theoretical references for additional research on its applications.

Experimental

Materials

The reagents used in this research are listed in Table 1 and applied without further purification.

TG experiments

The ramped temperature and isothermal TG experiments were performed using Pyris 1 (PerkinElmer, Shelton, Connecticut, USA) with platinum crucibles. The mass of the samples used in TG experiments was 8.0 ± 0.2 mg. Ramped temperature TG experiments were performed at 30.0–500.0 °C, with heating rates of 4.0, 8.0, 12.0, and 16.0 K min⁻¹ under a nitrogen flow rate of 20.0 mL min⁻¹. The dynamic TG curves were used to analyze the pyrolysis and pyrolysis kinetics of [Bmim][DBP]. Isothermal TG experiments were performed under a nitrogen atmosphere at fixed temperatures of 166.0, 170.0, 180.0, 190.0, and 200.0 °C for 24.0 h. Moreover, the obtained isothermal TG data were used to validate the long-term thermal stability of [Bmim][DBP].

GC/MS and FTIR spectrometers

The gaseous pyrolysis products of [Bmim][DBP] were analyzed using an Agilent 6890 N gas chromatograph equipped with an Agilent 5973 network mass selective detector (Agilent Technologies, California, USA) under a

helium atmosphere with a flow rate of 100.0 mL min⁻¹. The [Bmim][DBP] samples were maintained at 500.0 °C in a sealed vacuum tank, and the gaseous pyrolysis products were subsequently injected into the chromatograph by a syringe. Furthermore, the residual solid layers of [Bmim][DBP] were evaluated with a FTIR spectrometer (Spectrum 100).

LOI and UL-94 experiments

LOI tests were performed using an HC-2 oxygen index meter (Nanjing Jiangning Analytical Instrument Co., Ltd., Nanjing, China), and the dimensions of the measured specimen were 130.0 mm × 6.5 mm × 3.2 mm, as specified in ASTM D2863-77. Similarly, UL-94 tests were performed using a CZF-3 instrument (Nanjing Jiangning Analytical Instrument Co., Ltd., Nanjing, China), and the dimensions of the measured specimen were 130.0 mm × 13.0 mm × 3.2 mm, as specified in ASTM D3801.

Kinetic models

According to the recommendations of the Kinetics Committee of the International Confederation for the Thermal Analysis and Calorimetry, the pyrolysis process can be expressed as follows [25, 26]:

$$\frac{d\alpha}{dt} = kf(\alpha) \text{ or } G(\alpha) = kt \quad (1)$$

where t is the reaction time, α is the conversion degree at a specific time, $d\alpha/dt$ is the mass loss rate, and $f(\alpha)$ and $G(\alpha)$ are the differential and integral forms, respectively, of the mechanism function. The reaction rate constant k can be described as follows:

$$k = A \exp\left(-\frac{E_a}{RT}\right) \quad (2)$$

where A is the pre-exponential factor, T is the absolute temperature, E_a is the apparent activation energy, and R is the universal gas constant ($8.314 \text{ J mol}^{-1} \text{ K}^{-1}$).

Nonisothermal methods were used for the pyrolysis kinetic analysis of [Bmim][DBP]. The kinetic analysis methods used in this study were as follows:

Integral isoconversional method of Starink method [25, 27]:

$$\ln\left[\frac{\beta}{T^{1.92}}\right] = C - 1.0008 \times \frac{E_a}{R \times T} \quad (3)$$

where β is the heating rate, and C is a constant. E_a can be calculated from the slope of the plot of $\ln[\beta/(T^{1.92})]$ against $1000/T$.

Differential isoconversional method of Friedman method [28]:

Table 1 Information of reagents used in this research

Material	1-Butyl-3-methylimidazolium dibutyl phosphate	Bisphenol-A-based epoxy resin	Diethylenetriamine	Polypropylene glycol diglycidyl ether	Melamine
Abbreviation	[Bmim][DBP]	EP (E-44)	DETA	PPGDE	MA
Formula	C ₁₆ H ₃₃ N ₂ O ₄ P	–	C ₄ H ₁₃ N ₃	(C ₃ H ₆ O) _n ·C ₆ H ₁₀ O ₃	C ₃ H ₆ N ₆
Purity/%	96.0	–	99.8	–	99.0
Supplier	Shanghai Macklin Biochemical Technology Co., Ltd. (Shanghai, China)	Shandong Deyuan Epoxy Resin Co., Ltd. (Shandong, China)	Shanghai Lingfeng Chemical Reagent Co., Ltd. (Shanghai, China)	Shanghai Macklin Biochemical Technology Co., Ltd. (Shanghai, China)	Shanghai Lingfeng Chemical Reagent Co., Ltd. (Shanghai, China)

$$\ln \left[\frac{dx}{dt} \right]_{\alpha, i} = \ln [f(\alpha)A_i] - \frac{E_a}{R \times T_{\alpha, i}} \quad (4)$$

where the index i is introduced to denote various temperature programs. The value of E_a at each given α can be determined from the slope of a plot of $\ln(dx/dt)_{\alpha, i}$ against $1/T_{\alpha, i}$.

A model-free method, the compensation effect, was used to determine the accurate mechanism function. The method is described as follows [25]:

First, a model-fitting method of Coats-Redfern method [29] was used to obtain kinetic parameters of ($E_{a, i}$, A_i).

$$\ln \left[\frac{G(\alpha)}{T^2} \right] = \ln \frac{A_i \times R}{\beta \times T} - \frac{E_{a, i}}{R \times T} \quad (5)$$

The tentative functions of $G(\alpha)$ were substituted in Eq. (5), and the least squares fitting method was used to perform linear regression of $\ln[G(\alpha)/T^2]$ versus $1000/T$. Accordingly, $G(\alpha)$ was derived, and the corresponding kinetic parameters of ($E_{a, i}$, A_i) were obtained. However, because of the inherent flaws of the model-fitting method, the obtained $G(\alpha)$ was unreliable. Therefore, a compensation effect has been considered.

$$\ln A_0 = aE_0 + b \quad (6)$$

The aforementioned kinetic parameters of ($E_{a, i}$, A_i) were used to determine the parameters of a and b . Subsequently, the average value of the model-free apparent activation energy (E_0) was substituted in Eq. (6), and the pre-exponential factor A_0 was estimated.

Then, an integral form was used to numerically reconstruct the mechanism function.

$$G(\alpha) = \frac{A_0 T_x}{\beta} \int_0^{\alpha} \exp \left(\frac{-E_0}{R \times T} \right) dT \quad (7)$$

where T_x is the temperature corresponding to a given α . A set of numerical values of $G(\alpha)$ at different values of α was obtained using Eq. (7). Therefore, an analytical form of the mechanism function was established by plotting the

numerical $G(\alpha)$ values. Subsequently, the most suitable matching mechanism function was selected through comparison against the theoretical dependencies.

Finally, the Málek method was used to verify the reliability of derived $G(\alpha)$ [30, 31].

$$y_1(\alpha) = \frac{f(\alpha) \times g(\alpha)}{f(0.5) \times g(0.5)} \quad (8)$$

$$y_2(\alpha) = \left(\frac{T}{T_{0.5}} \right)^2 \times \left(\frac{\frac{dx}{dt}}{\left(\frac{dx}{dt} \right)_{0.5}} \right) \quad (9)$$

where $y_1(\alpha)$ and $y_2(\alpha)$ are defined as the standard and experimental curves, respectively. The proposed mechanism function can be substituted in Eq. (8), and the experimental data can be fitted to Eq. (9). Therefore, an accurate $f(\alpha)$ can be determined by comparing the consistency between the standard and experimental curves.

Results and discussion

Dynamic TG analysis

Figure 1a presents the ramped temperature TG and DTG curves of [Bmim][DBP] at heating rates of 4.0, 8.0, 12.0, and 16.0 K min⁻¹. The changes in the curves of TG at different heating rates were clearly consistent. Considering the TG curve corresponding to the heating rate of 4.0 K min⁻¹ as an example, three relatively discrete stages in the decomposition process were discernible in the entire TG curve. The first stage occurred between 30.0 and 125.0 °C (± 5.0 °C; Fig. 1b), which resulted in the vaporization of moisture and residual reactant from the sample. The second stage was identified as the dominant stage in the decomposition; it occurred between 247.0 and 318.0 °C (± 5.0 °C; Fig. 1c) and corresponded to the active pyrolysis of [Bmim][DBP]. The final stage occurred between 318.0 and 450.0 °C (± 5.0 °C) and was

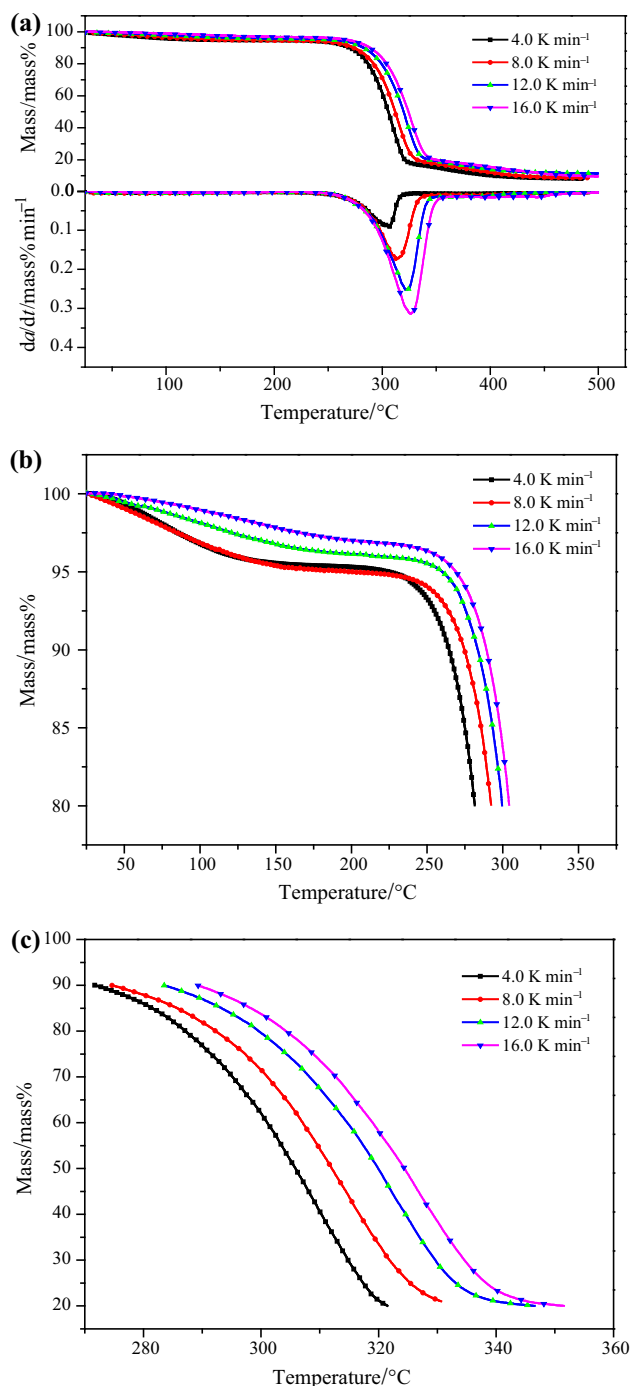


Fig. 1 **a** Ramped temperature TG and DTG curves of [Bmim][DBP] at heating rates of 4.0, 8.0, 12.0, and 16.0 K min⁻¹. **b** A zoom of the decomposition of [Bmim][DBP] from 80.0 to 100.0% at heating rates of 4.0, 8.0, 12.0, and 16.0 K min⁻¹. **c** A zoom of main degradation of [Bmim][DBP] from 10.0 to 90.0% at heating rates of 4.0, 8.0, 12.0, and 16.0 K min⁻¹

characterized by the decomposition of the phosphate-containing products of [Bmim][DBP]. However, the pyrolysis of the partial products may also have occurred in the second stage. Therefore, the temperature ranges of pyrolysis

process were only defined for the convenience of the subsequent analysis. Typically, these features of the decomposition process (identified at a heating rate 4.0 K min⁻¹) were also observed at other heating rates.

The apparent onset decomposition temperature of [Bmim][DBP] was identified as the point of intersection of the baseline mass and the tangent to the TG curve as the decomposition occurs [32]. The T_0 values derived from the dynamic TG/DTG curves were 275.2, 285.6, 292.9, and 297.3 °C (± 0.5 °C) at heating rates of 4.0, 8.0, 12.0, and 16.0 K min⁻¹, respectively. The T_0 values increased from 275.2 to 297.3 °C (± 0.5 °C), and the decomposition curves shifted to higher temperatures with an increase in the heating rate. The maximum [Bmim][DBP] decomposition rate and the corresponding temperature, determined using the DTG curves, increased when the heating rate increased. This phenomenon may be ascribed to the limited heat transfer when a high heating rate was used, given that a high heating rate reduced the total heating time; thus, lower temperatures were maintained for a relatively short duration [33, 34].

The T_0 value obtained using dynamic thermal analysis is commonly used as an indicator of the short-term thermal stability of ILs. Moreover, the carbon-forming property of [Bmim][DBP], which was described by the mass fraction of residual carbon, has also been analyzed through TG experiments. The mass fractions of residual carbon of [Bmim][DBP] were 8.6%, 9.3%, 9.6%, and 10.2% ($\pm 0.1\%$) at heating rates of 4.0, 8.0, 12.0, and 16.0 K min⁻¹, respectively. The formation of residual carbon might occur mainly because of the presence of phosphorus in the anion of [Bmim][DBP]. Therefore, ramped temperature TG revealed that [Bmim][DBP] exhibits high thermal stability and favorable carbon-forming properties.

Pyrolysis kinetics analysis

Determination of E_a and A

Apart from the apparent onset decomposition temperature, the apparent activation energy was a crucial and effective indicator of the thermal stability of [Bmim][DBP]. E_a was calculated using the Starink and Friedman methods at various conversion fractions (α). The TG/DTG tests revealed that the dominant pyrolysis process occurred at conversion fractions of approximately 10.0–80.0%. The E_a was calculated for experiments at heating rates of 4.0, 8.0, 12.0, and 16.0 K min⁻¹ and a single α . The fitting curves determined using the two models at various conversion factors were notably similar. The E_a values obtained using the two methods at the various conversion fractions were similar (Table 2). Taking the results of the Starink method

Table 2 E_a values obtained using two methods and different conversion fractions

Conversion/mass%	10.0	20.0	30.0	40.0	50.0	60.0	70.0	80.0
Starink method								
$E_a/\text{kJ mol}^{-1}$	158	152	157	159	160	161	163	153
R^2	0.9945	0.9993	0.9994	0.9988	0.9970	0.9979	0.9978	0.9928
Friedman method								
$E_a/\text{kJ mol}^{-1}$	159	155	159	160	160	162	164	156
R^2	0.9938	0.9992	0.9993	0.9986	0.9966	0.9976	0.9976	0.9918

The standard deviation of E_a calculated by two methods was $\pm 2 \text{ kJ mol}^{-1}$

as an example, the example of E_a at $\alpha = 10.0\%$ was $157.59 \pm 1.50 \text{ kJ mol}^{-1}$, which was slightly greater than that at $\alpha = 20.0\%$; this indicated that the initiation of pyrolysis required a high energy input to overcome the energy barrier. Thus, the apparent activation energy increased with an increase in the conversion fraction. The E_a reduced substantially at a conversion fraction of 80.0%, probably because of the third stage of pyrolysis when the pyrolysis of partial products occurred. Moreover, the value of E_a calculated using the Friedman method was slightly higher than calculated using the Starink method; however, the changes in both trends were consistent for the values obtained using both methods. Assuming the conversion fractions 10.0–70.0% in the main degradation step, E_a values calculated by the Starink and Friedman methods were 152–163 kJ mol^{-1} ($\pm 2 \text{ kJ mol}^{-1}$) and 155–163 kJ mol^{-1} ($\pm 2 \text{ kJ mol}^{-1}$), respectively. Notably, the regression coefficients (R^2) of all fitting curves exceeded 0.99. [Bmim][DBP] exhibited a higher value of E_a than did similar ILs such as [Bmim][Cl] or [Bmim][NTf₂] [1, 35]. Therefore, [Bmim][DBP] was concluded to have excellent thermal stability because of its high apparent activation energy.

The pre-exponential factor A of [Bmim][DBP] was determined using the following assumption [25]:

$$A = \frac{\beta \times E_a}{R \times T_p^2} \times \exp\left(\frac{E_a}{R \times T_p}\right) \quad (10)$$

Therefore, A at a specified β could be estimated through the obtained E_a and T_p . According to Table 2, the value of E_a calculated using the two methods did not vary

significantly with different α . Therefore, the mean of E_a ($159 \pm 2 \text{ kJ mol}^{-1}$) at 10.0–70.0% calculated using the Starink method was used to estimate A at different β . Subsequently, $\ln A$ of [Bmim][DBP] was calculated to be $27.7 \pm 0.4 \text{ s}^{-1}$ at the heating rates 4.0, 8.0, 12.0, and 16.0 K min^{-1} .

Determination of $f(\alpha)$

According to the value of E_a calculated using the Starink and Friedman methods, the variation in the values of E_a at 10.0–70.0% with α was negligible. Therefore, the most probable kinetic function of [Bmim][DBP] during the dominant thermal pyrolysis process could be estimated by following some analytical steps. First, a probable mechanism function of $G(\alpha) = -\ln(1 - \alpha)$ was proposed using the Coats-Redfern method. The kinetic parameter of $E_{\alpha, i}$ was relatively close to E_0 ($159 \pm 2 \text{ kJ mol}^{-1}$; the average value of E_a obtained using the Starink method) and is listed in Table 3. The values of ($E_{\alpha, i}, A_i$) were then introduced in Eq. (6), and the relationship of the compensation effect was observed as follows:

$$\ln A_0 = 0.2238E_0 - 7.9720 \quad (11)$$

According to Eq. (11), $\ln A_0$ corresponding to E_0 was calculated to be 27.5 s^{-1} , which most closely matched the pre-exponential factor value, $\ln A$, obtained using Eq. (10). Subsequently, the determined E_0 and A_0 were substituted into Eq. (7) and the mechanism function in integral form was numerically reconstructed. Therefore, numerical values of $G(\alpha)$ corresponding to different values of α were obtained; they are depicted in Fig. 2. The variation of analytical $G(\alpha)$

Table 3 Kinetic parameters of (E_i, A_i) based on $G(\alpha) = -\ln(1 - \alpha)$ at heating rates of 4.0, 8.0, 12.0, and 16.0 K min^{-1} and the estimated relationship of compensation effect

Model $G(\alpha) = -\ln(1 - \alpha)$	Heating rate/ K min^{-1}					$\ln A_0 = aE_0 + b$	
	4.0	8.0	12.0	16.0	Average	a	b
$E_i/\text{kJ mol}^{-1}$	132	135	141	146	138.5	0.2238	- 7.972
$\ln A_i/\text{s}^{-1}$	21.5	22.2	23.5	24.8	23.0		

The standard deviations of E_0 and $\ln A_0$ were $\pm 2 \text{ kJ mol}^{-1}$ and $\pm 0.4 \text{ s}^{-1}$, respectively

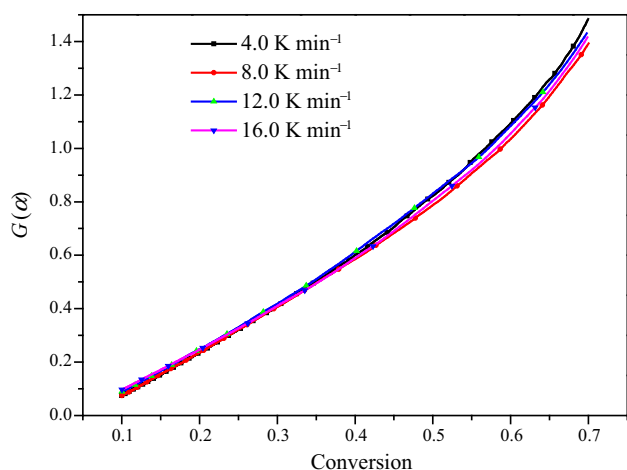


Fig. 2 Analytical $G(\alpha)$ plots for the mechanism function $G(\alpha) = -\ln(1 - \alpha)$ at heating rates of 4.0, 8.0, 12.0, and 16.0 K min^{-1}

plots was negligible as β increased. The most suitably matched model was identified to be $G(\alpha) = -\ln(1 - \alpha)$ through a comparison of analytical plots against theoretical dependence [25]. Finally, the kinetic model was substituted into the equation of the Málek method for comparing the resultant curves with the experimental data (Fig. 3). As illustrated in Fig. 3, the standard curves were consistent with the experimental data for $10.0\% \leq \alpha \leq 70.0\%$ but they substantially deviated in $70.0\text{--}80.0\%$ range. These deviations indicated that partial products were pyrolyzed before the temperature reached 318.0 ± 5.0 °C, and they also confirmed that the decrease in E_a at $\alpha = 80.0\%$ most likely resulted from the pyrolysis of the partial products. Therefore, the kinetic model of $G(\alpha) = -\ln(1 - \alpha)$ was determined to be the most probable mechanism function of [Bmim][DBP]. Furthermore, the

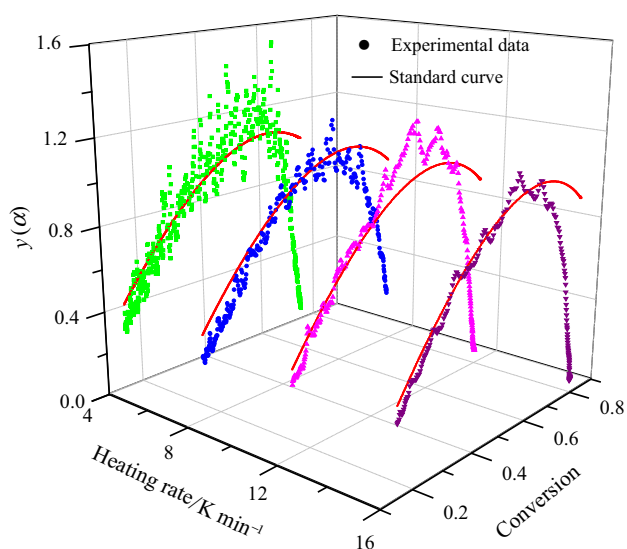


Fig. 3 Comparison curves of the Málek method with kinetic function $f(\alpha) = 1 - \alpha$ at heating rates of 4.0, 8.0, 12.0, and 16.0 K min^{-1}

proposed kinetic model could be helpful to analyze the flame-retardant mechanism of [Bmim][DBP] for use in polymers.

Long-term thermal stability analysis

A conventional characterization parameter, T_0 , derived using ramped TG overestimated the true thermal stability of [Bmim][DBP]. Based on the ramped temperature TG results, 24.0 h isothermal TG of [Bmim][DBP] at 170.0, 180.0, 190.0, and 200.0 °C was performed, as depicted in Fig. 4. Although the apparent onset decomposition temperature of [Bmim][DBP] was 289.9 ± 0.5 °C, Fig. 4 shows that mass loss also occurred at temperatures of 170.0–200.0 °C during 24.0 h isothermal TG. In particular, the mass loss of [Bmim][DBP] exceeded 10.0% at the isothermal temperature of 200.0 °C for 24.0 h. Therefore, the temperature for long-term thermal stability of [Bmim][DBP] was considerably lower than that for short-term thermal stability, and this observation was consistent with previous reports [36]. Thus, this study proposed the MOT, which specifies the long-term thermal stability of ILs that may be used for prolonged periods. Furthermore, an empirical model, which uses the parameters derived from a short-term dynamic analysis, was introduced to predict the MOT. The model can be expressed as follows [20]:

$$\text{MOT} = \frac{E_a}{R \times \{-\ln[\ln(\frac{m_a}{m})] + \ln(A \times t_{\max})\}} \quad (12)$$

where t_{\max} is the maximum time for which the IL is stable at the calculated MOT, m is the residual mass, and m_0 is the initial mass. E_a and A can be calculated through short-term dynamic analysis. For guidance in engineering applications, the effective MOT is defined as the temperature at which the [Bmim][DBP] mass loss is less than

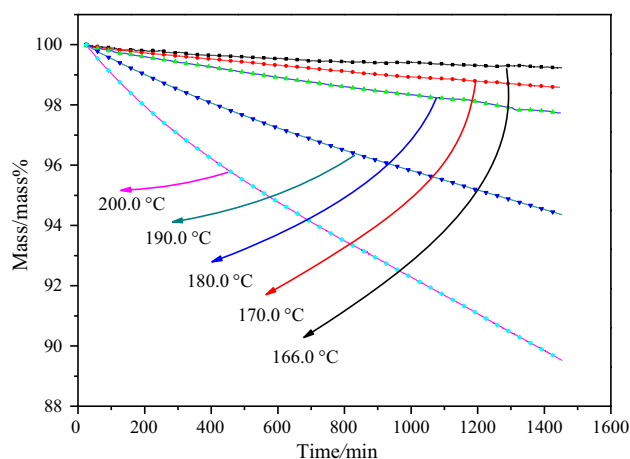


Fig. 4 Isothermal TG curves in the temperature range of 166.0–200.0 °C

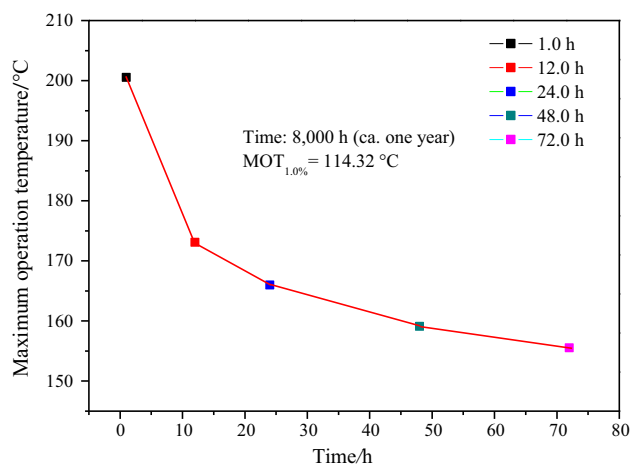


Fig. 5 Calculated values of $MOT_{1.0\%}$ after different time durations

1.0% over the time t_{max} . Equation (12) can then be modified as follows [22]:

$$MOT_{1.0\%} = \frac{E_a}{R \times [4.6 + \ln(A \times t_{max})]} \quad (13)$$

The $MOT_{1.0\%}$ at different time points calculated using Eq. (13) is illustrated in Fig. 5. The predicted MOT at 24.0 h was 166.0 ± 0.2 °C. Figure 4 confirms that the mass loss of [Bmim][DBP] under the isothermal temperature of 166.0 ± 0.2 °C was approximately equal to 1.0%. Thus, the predicted MOT was consistent with the experimental result obtained through isothermal TG. This consistency also somewhat demonstrated the accuracy of the calculated E_a and A values. Therefore, the empirical model is an accurate, effective, and convenient method for predicting the long-term thermal stability of [Bmim][DBP]. As Fig. 5 indicates, the MOT of [Bmim][DBP] after 1.0, 12.0, 24.0, 48.0, and 72.0 h was 200.6, 173.1, 166.0, 159.1, and 155.5 °C (± 0.2 °C), respectively. In addition, the MOT after a longer period of 8000 h was calculated to be 114.3 ± 0.2 °C. These calculated MOT values were considerably lower than the calculated T_0 values, and the long-term thermal stability decreased with an increase in isothermal duration. Therefore, the desired operating temperature can be adjusted by altering the operation duration. For example, the melt-blending process for preparing the epoxy resin and [Bmim][DBP] composite can be performed at 173.1 ± 0.2 °C if the process must be conducted for 12.0 h.

Decomposition product analysis

The application of [Bmim][DBP] as a flame retardant for polymers is largely affected by the decomposition products of ILs, which should be nontoxic and nonpolluting. According to the TG results, most [Bmim][DBP]

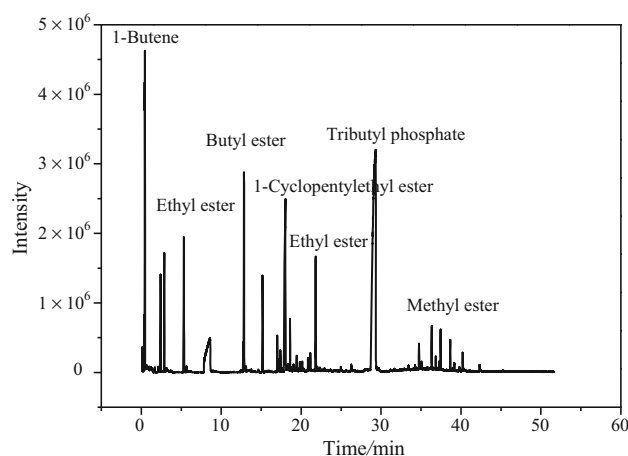


Fig. 6 Typical mass spectra of the gaseous products of [Bmim][DBP] by GC/MS

decomposition products were released in the gaseous form, with only a minute amount of residual solid. The gaseous products and residual solids were analyzed through GC/MS and FTIR spectrometers, respectively.

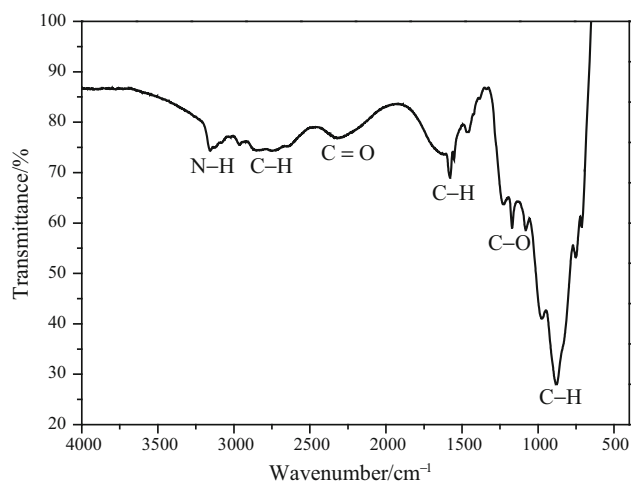
The typical mass spectra of the gaseous products of [Bmim][DBP] are presented in Fig. 6, and the main analysis results are listed in Table 4. The gaseous constituent analysis mainly revealed the following. First, a series of alkyl or alkenyl groups with a carbon chain length of 1–4 was detected. The methyl and butyl signals were directly generated by the pyrolysis of [Bmim][DBP], and the remainder probably resulted from cracking at elevated temperatures or from being broken during the GC/MS of butyl chains. Second, 1 H-imidazole ([Him]⁺), methyl imidazole ([Mim]⁺), and 3-methyl-1 H-imidazole ([MHim]⁺) were detected at m/z values of 68, 82, and 83, respectively. The imidazole cations may have been produced by parallel pathways of degradation of [Bmim][DBP], and the imidazolium rings might eventually be degraded into other micromolecules. Finally, a macromolecule of tributyl phosphate and related esters (methyl ester, ethyl ester, and butyl ester) were detected. Moreover, free radicals of phosphorus oxygen were produced during pyrolysis, indicating that [Bmim][DBP] can act as a gas-phase flame retardant.

The FTIR spectra of the residual solids of [Bmim][DBP] have several major absorption peaks (Fig. 7). The residuals were mainly produced by the carbonization of phosphoric acid free radicals at a certain temperature. The peak at 875 cm^{-1} was assumed to be that of the C–H groups, which may have been derived from the imidazolium rings. However, the C–H groups corresponding to peaks at 1578 and 2731 cm^{-1} were separately derived from the butylene and ester groups. Moreover, the peaks at 1170 , 2321 , and 3153 cm^{-1} were assigned to the C–O, C=O, and N–H

Table 4 Main analysis results of gaseous products, as determined through GC/MS

PK	RT/min	Database	Formula	Ref.	Qual.
1	1.503	1-Butene	C ₄ H ₈	172	9
		1-Propene	C ₃ H ₆	182	9
		2-Methyl-1-butene	C ₅ H ₁₀	173	9
2	1.654	2-Pentene	C ₅ H ₁₀	548	59
		(E)-Cyclopropane	C ₃ H ₄	566	45
		1,1-Dimethyl-2-pentene	C ₇ H ₁₄	540	42
3	2.922	Butanoic acid	C ₄ H ₈ O ₂	4206	86
		Methyl ester	C ₂ H ₄ O ₂	4205	78
4	4.093	Ethyl ester	C ₃ H ₆ O ₂	41434	25
5	4.380	Propanoate	C ₃ H ₆ O ₂	21057	64
6	7.647	Butane	C ₄ H ₁₀	13311	33
7	10.405	1 H-imidazole	C ₃ H ₄ N ₂	1128	90
		3-Methyl-1 H-imidazole	C ₄ H ₆ N ₂	1123	72
8	13.615	Propanoic acid	C ₃ H ₆ O ₂	20188	83
		Butyl ester	C ₅ H ₁₀ O ₂	57075	83
		Butanoic acid	C ₄ H ₈ O ₂	68383	83
9	18.311	Phenol	C ₆ H ₆ OH	16183	62
		4-Methoxy-benzenemethanamine	C ₉ H ₁₃ NO	16195	50
10	19.060	1-Cyclopentylethyl ester	C ₉ H ₁₆ O ₂	82340	37
11	21.012	Pentyl ester	C ₆ H ₁₂ O ₂	51083	46
		Heptyl ester	C ₈ H ₁₆ O ₂	71157	46
12	24.970	2-Amino-2-oxo-acetic acid	C ₃ H ₅ O ₃ N	71888	37
		Ethyl ester	C ₃ H ₆ O ₂	82773	32
13	28.929	Tributyl phosphate	(C ₄ H ₉) ₃ PO ₄	102223	83
14	34.252	2-Amino-1-methyl-cyclohexane	C ₇ H ₁₅ N	21622	25
15	35.069	Methyl ester	C ₂ H ₄ O ₂	105646	90

PK peak of GC/MS, RT retention time, Ref reference number, Qual quality

**Fig. 7** FTIR spectra of residual solids of [Bmim][DBP] pyrolysis

groups, respectively. The C–O and N–H groups may have been derived from the ester and [Him]⁺ groups that were formed during pyrolysis, whereas the C=O group may have

been derived from carbonates because of the mixed air atmosphere during pyrolysis. Moreover, some lower-wavelength peaks were present in the FTIR spectra, such as that at 1044 cm⁻¹ corresponding to the P=O group, which was mainly derived from the phosphorous compounds. Thus, the IL [Bmim][DBP] has high carbonization performance and excellent flame-retardant properties in its condensed phase.

Flame-retardant capacity analysis

To analyze the flame-retardant capacity of [Bmim][DBP], a modified composite of EP/[Bmim][DBP] was prepared and tested by LOI and UL-94 experiments. The flame resistances of EP/[Bmim][DBP] composites are listed in Table 5. The composite of EP with 10.0% MA was also tested to serve as a reference. The lowest LOI (19.4) and UL-94 (NR) indicated the high flammability of pure EP. As can be inferred, the addition of [Bmim][DBP] distinctly increased the LOI and upgraded the UL-94 to V-1 level, meaning that [Bmim][DBP] considerably improved the

Table 5 Flame resistance of EP composites determined using LOI and UL-94 tests

Sample	Pure EP	EP composites			
		5.0% [Bmim][DBP]	10.0% [Bmim][DBP]	15.0% [Bmim][DBP]	5.0% MA
LOI test	19.4	21.6	22.9	24.0	22.1
UL-94 test	NR	V-1	V-1	V-1	V-1

NR no rating

flame resistance of EP. Moreover, the flame resistance (LOI as indicator) of EP composite was increased with the increase in [Bmim][DBP] concentration. Particularly, the LOI reached 22.9 when 10.0% [Bmim][DBP] was added, which corresponds to that of a self-extinguishing material [37]. By comparison, the LOI of 10.0% EP/[Bmim][DBP] was slightly higher than that of 10.0% EP/MA. Furthermore, the UL-94 of EP/MA was V-2 level and lower than that at the V-1 level of EP/[Bmim][DBP]. Therefore, [Bmim][DBP] has an acceptable flame-retardant capacity and is superior to MA.

Conclusions

The thermal stability, pyrolysis kinetics, decomposition products, and flame-retardant capacity of [Bmim][DBP] were investigated through TG, GC/MS, FTIR, LOI, and UL-94. First, ramped TG revealed the apparent onset decomposition temperature to be 275.2–297.3 °C (± 0.5 °C) and the mass fraction of residual carbon to be 8.6–10.2% ($\pm 0.1\%$), indicating that [Bmim][DBP] has the desired thermal stability and carbon-forming ability. Second, according to obtained kinetic triplets, the thermal decomposition kinetic model should be established as: $\frac{dz}{dt} = \exp\left(27.7 - \frac{158 \times 10^3}{RT}\right) \times (1 - \alpha)$. The long-term thermal stability was then analyzed using isothermal TG, and the MOT for various experimental durations was estimated using an empirical equation. Furthermore, the analysis of decomposition products suggested that [Bmim][DBP] acts as a flame retardant mainly in its condensed phase and slightly in its gas phase. Finally, the flame-retardant tests verified that [Bmim][DBP] effectively improved the flame resistance of epoxy resin. Therefore, results revealed that [Bmim][DBP] is an applicable flame retardant for use in polymers.

Acknowledgements This study was very grateful to be supported by the Process Safety and Disaster Prevention Laboratory, Postgraduate Research and Practice Innovation Program of Jiangsu Province (KYCX17_0915). The authors appreciate the original suggestions and heartfelt inspiration for provided by the members of IL research groups.

References

- Maton C, Vos N, Stevens CV. Ionic liquid thermal stability: decomposition mechanism and analysis tools. *Chem Soc Rev*. 2013;42:5963–77.
- Zheng L, Bu XX, Fan BH, Wei J, Xing NN, Guan W. Study on thermodynamic property for ionic liquid [C4mim][Lact] (1-butyl-3-methylimidazolium lactic acid). *J Therm Anal Calorim*. 2016;123:1619–25.
- Kroon MC, Buijs W, Peters CJ, Witkamp GJ. Quantum chemical aided prediction of the thermal decomposition mechanism and temperature of ionic liquids. *Thermochim Acta*. 2007;465:40–7.
- Tang G, Deng D, Chen J, Zhou KQ, Zhang H, Huang XJ, Zhou ZJ. The influence of organo-modified sepiolite on the flame-retardant and thermal properties of intumescent flame-retardant polylactide composites. *J Therm Anal Calorim*. 2017;130:763–72.
- Tang S, Qian LJ, Liu XX, Dong YP. Gas-phase flame-retardant effects of a bi-group compound based on phosphaphenanthrene and triazine-trione groups in epoxy resin. *Polym Degrad Stab*. 2016;133:350–7.
- Zhang L, Wang YC, Liu Q, Cai XF. Synergistic effects between silicon-containing flame retardant and DOPO on flame retardancy of epoxy resins. *J Therm Anal Calorim*. 2016;123:1343–50.
- Wang YH, Zhang S, Wu XM, Lu CL, Cai YQ, Ma LJ, Shi G, Yang LT. Effect of montmorillonite on the flame-resistant and mechanical properties of intumescent flame-retardant poly(-butylene succinate) composites. *J Therm Anal Calorim*. 2017;128:1417–27.
- Xu JZ, He ZM, Wu WH, Ma HY, Xie JX, Qu HQ, Jiao YH. Study of thermal properties of flame retardant epoxy resin treated with hexakis[p-(hydroxymethyl)phenoxy]cyclotriposphazene. *J Chem Anal Calorim*. 2013;114:1341–50.
- Chen SJ, Wang CL, Li J. Effect of alkyl groups in organic part of polyoxometalates based ionic liquids on properties of flame retardant polypropylene. *Thermochim Acta*. 2016;631:51–8.
- Yang XF, Ge NL, Hu LY, Gui HG, Wang ZG, Ding YS. Synthesis of a novel ionic liquid containing phosphorus and its application in intumescent flame retardant polypropylene system. *Polym Adv Technol*. 2013;24:568–75.
- Chen SJ, Li J, Zhu YK, Guo ZB, Su SP. Increasing the efficiency of intumescent flame retardant polypropylene catalyzed by polyoxometalate based ionic liquid. *J Mater Chem A*. 2013;48:15242–6.
- Sorai M. *Comprehensive handbook of calorimetry and thermal analysis*. Chichester: Wiley; 2004.
- Ullah Z, Bustam MA, Man Z, Khan AS. Thermal stability and kinetic study of benzimidazolium based ionic liquid. *Procedia Eng*. 2016;148:215–22.
- Kamavaram V, Reddy RG. Thermal stabilities of di-alkylimidazolium chloride ionic liquids. *Int J Therm Sci*. 2007;47:773–7.

15. Muhammad A. Thermal and kinetic analysis of pure and contaminated ionic liquid: 1-butyl-2, 3-dimethylimidazolium chloride (BDMIMCl). *Pol J Chem Technol*. 2016;18:122–5.
16. Heym F, Etzold BJM, Kern C, Jess A. An improved method to measure the rate of vaporization and thermal decomposition of high boiling organic and ionic liquids by thermogravimetric analysis. *Phys Chem Chem Phys*. 2010;12:12089–100.
17. Abusaidi H, Ghaieni HR. Thermal analysis and kinetic decomposition of nitro-functional hydroxyl-terminated polybutadiene bonded explosive. *J Chem Anal Calorim*. 2017;127:2301–6.
18. Golofit T, Zielenkiewicz T. The influence of substituents position on products of dinitrotoluene isomers initial thermal decomposition. *J Chem Anal Calorim*. 2017;128:311–7.
19. Chen Y, Cao YY, Shi Y, Xue ZM, Mu TC. Quantitative research on the vaporization and decomposition of [EMIM][Tf₂N] by thermogravimetric analysis–mass spectrometry. *Ind Eng Chem Res*. 2012;51:7418–27.
20. Seeburger A, Andresen AK, Jess A. Prediction of long-term stability of ionic liquids at elevated temperatures by means of non-isothermal thermogravimetric analysis. *Phys Chem Chem Phys*. 2009;11:9375–81.
21. Navarro P, Larriba M, Rojo E, Garcia J, Rodríguez F. Thermal properties of cyano-based ionic liquid. *J Chem Eng Data*. 2013;58:2187–93.
22. Efimova A, Pfützner L, Schmidt P. Thermal stability and decomposition mechanism of 1-ethyl-3-methylimidazolium halides. *Thermochim Acta*. 2015;604:129–36.
23. Mohamed MA, Attia AK. Thermal behavior and decomposition kinetics of cinnarizine under isothermal and non-isothermal conditions. *J Chem Anal Calorim*. 2017;127:1751–6.
24. Sun DC, Yao YW. Synthesis of three novel phosphorus-containing flame retardants and their application in epoxy resins. *Polym Degrad Stab*. 2011;96:1720–4.
25. Vyazovkin S, Burnham AK, Criado JM, Pérez-Maqueda LA, Popescu C, Sbirrazzuoli N. ICTAC Kinetics Committee recommendations for performing kinetic computations on thermal analysis data. *Thermochim Acta*. 2011;520:1–19.
26. Vyazovkin S, Chrissafis K, Lorenzo ML, Koga N, Pijolat M, Roduit B, Sbirrazzuoli N, Suñol JJ. ICTAC Kinetics Committee recommendations for collecting experimental thermal analysis data for kinetic computations. *Thermochim Acta*. 2014;590:1–23.
27. Starink MJ. The determination of activation energy from linear heating rate experiments: a comparison of the accuracy of iso-conversion methods. *Thermochim Acta*. 2003;404:163–76.
28. Friedman HL. Kinetics of thermal degradation of char-forming plastics from thermogravimetry: application to a phenolic plastic. *J Polym Sci Part C*. 1964;6:183–95.
29. Coats AW, Redfern JP. Kinetic parameters from thermogravimetric data. *Nature*. 1964;201:68–9.
30. Málek J, Smrčka V. The kinetic analysis of the crystallization processes in glasses. *Thermochim Acta*. 1991;186:153–69.
31. Málek J. A computer program for kinetic analysis of non-isothermal thermos-analytical data. *Thermochim Acta*. 1989;138:337–46.
32. Muhammad A, Mutalib AMI, Wilfred CD, Murugesan T, Shafeeq A. Thermophysical properties of 1-hexyl-3-methyl imidazolium based ionic liquids with tetrafluoroborate, hexafluorophosphate and bis(trifluoromethylsulfonyl)imide anions. *J Chem Therm*. 2008;40:1433–8.
33. Khan AS, Man Z, Bustam MA, Kait CF, Ullah Z, Nasrullah A, Khan MI, Gonfa G, Ahmad P, Muhammad N. Kinetics and thermodynamic parameters of ionic pretreated rubber wood biomass. *J Mol Liq*. 2016;223:754–62.
34. Karolina K, Beata G, Grzegorz G, Artur B, Zaneta KK. Thermal decomposition of binder based on etherified starch to use in foundry industry. *J Therm Anal Calorim*. 2017;130:285–90.
35. Parajó JJ, Teijeira T, Fernández J, Salgado J, Villanueva M. Thermal stability of some imidazolium [NTf₂] ionic liquid: isothermal and dynamic kinetic study through thermogravimetric procedures. *J Chem Thermodyn*. 2017;112:105–13.
36. Salgado J, Villanueva M, Parajó JJ, Fernández J. Long-term thermal stability of five imidazolium ionic liquids. *J Chem Thermodyn*. 2013;65:184–90.
37. Shen MY, Kuan CF, Kuan SC, Chen CH, Wang JH, Yip MC, Chiang CL. Preparation, characterization, thermal, and flame-retardant properties of green silicon-containing epoxy/functionalized graphene nanosheets composites. *J Nanomater*. 2013;2013:363–71.

Publisher's Note Springer Nature remains neutral with regard to jurisdictional claims in published maps and institutional affiliations.